T.A. van Walsum, s1869647
Master project
1-7-2013

Supervisors: E.J. Stamhuis & D.E. Worst

PENGUIN FLIPPER HYDRODYNAMICS

Do steady or unsteady hydrodynamic effects determine flow over the Adélie penguin (Pygoscelis adeliae) flipper? Using quantative flow analysis with laser sheet digital particle image velocimetry.

ABSTRACT

Leading Edge Vortices are a part of unsteady hydrodynamics, they allow an increase in lift and postpone stall effects. A recent study discovered LEV formation in swifts (*Apus apus*), broadening the possibilities for LEVs to be present in other birds as well.
A self-designed downscaled Adélie penguin flipper (base hydrofoil: NACA 63-018) was tested in a rotating system at three base velocities. The flipper was tested at angles of attack ranging from 0 ˚C up to 32.5 ˚C (with steps of 2.5 ˚C). PIVlab analysis allowed calculation of the particle displacement (vector analysis), created by the Adélie penguin flipper. Further analysis provided circulation around the penguin flipper at every angle of attack and base rotation velocity.
Our data reveals the presence of LEVs. The LEVs increased the Adélies' lift up to a maximum of 3.64. This is a significant increase in lift coefficient compared to expected lift value of a 2D model NACA 63-018 profile ($C_{L\,max}$ 1.20). Our increase in lift coefficient is non-linear to angle of attack and steeper than Javafoil's expected values. We conclude that our downscaled Adélie penguin flipper depicts the presence of LEV lift enhancement during rotational flight.

Keywords: *Pygoscelis adeliae, Penguin flipper, Unstable hydrodynamics, DPIV, Leading Edge Vortices, Lift Coefficient, Java-foil 2D analysis.*

INTRODUCTION

Penguins are unable to perform aerial flight, but are capable of remarkable underwater flight due to their flippers. The flippers are key to understanding their underwater locomotion (*Hui 1988a,b, Lovvorn & Liggins 2002*). Their swimming-method is lift-based combined with a high mechanic efficiency rate (>79%) (*Weihs & Webb 1983, Jackson, Locke & Brown 1992, Fish 1993, Fish 2000*). Adélie penguins have extraordinary fishing skills, rarely missing a target, and regularly seen burst swimming in order to catch their prey (*Ito et al. 2003, Watanabe & Takahashi 2013*). This shows that they are able to reach rather high swimming speeds; they may need the extra propulsion coming with unsteady flow phenomena during lift production of their flapping flippers.
Many studies, thus far, have focused on the hydrodynamics of the penguin body (*Bilo & Nachtigall 1980, Lovvorn et al. 2001*, *Lovvorn 2001*), and have revealed the highly hydrodynamic shape of its body(*Clark & Bemis 1979, Bannasch 1997*).

Culik et al. 1994 determined that this hydrodynamic shape yields a (*Pygoscelis adeliae*) drag coefficient that is significantly smaller than a perfect spindle ($C_{D\ Adélie}$: 0.0368, $C_{D\ perfect\ spindle}$: 0.04).
As for the flippers themselves, they have yet to be studied. How do their flippers affect the penguins' swimming abilities?

Two types of hydrodynamics exist with respect to flow around wing structures; steady and unsteady hydrodynamics. When the oncoming flow remains attached to wing, following the outline of the hydrofoil from leading edge to trailing edge, then steady hydrodynamics are at play. If the angle of attack, AOA (the angle at which the centered line of the wing is set to the oncoming flow), remains within a certain range, then attached flow (steady hydrodynamics) can be maintained. The range of available AOA depends strongly on the shape of the leading edge of the hydrofoil.

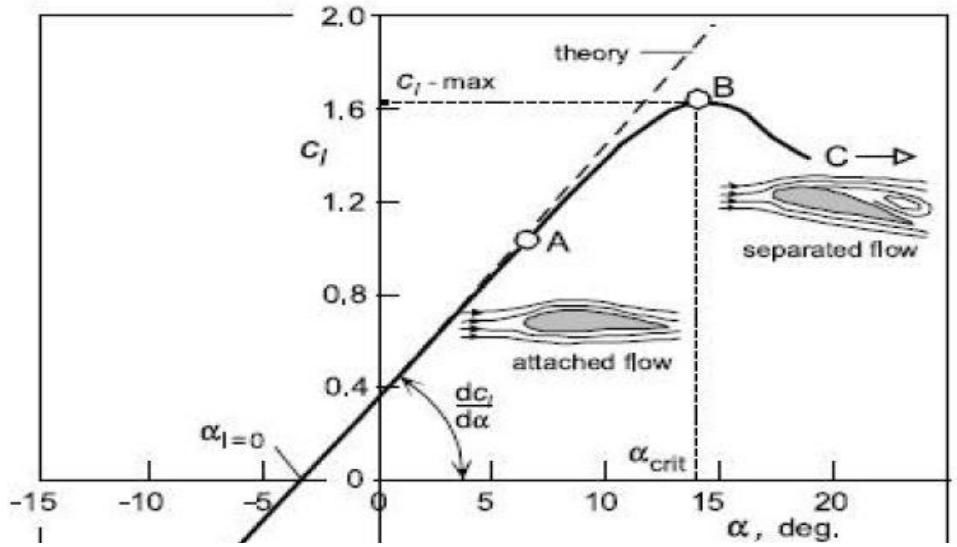

Figure 1. *Showing attached and separated flow on a 2-D hydrofoil. It's increase in lift occurs linearly over increase in angle of attack, up until the increase in drag starts taking effect. From: Torenbeek & Wittenberg 2009, NACA 4412 2D hydrofoil at Re: $9{\cdot}10^6$. In theory Lift coefficient should continue to increase linearly as angle of attack increases, in practice however, an increase in angle of attack only permits increase in lift coefficient up until critical angle of attack is reached (source: Canfield 2009).*

However, once a critical AOA is reached, beyond the steady AOA range, the flow will separate from the wing. In such case, the oncoming flow can no longer outline the hydrofoil as it would during steady hydrodynamics. In which case a vortex is formed at the leading edge and the wing experiences an increase in stalling (*Figure 1*).

Unsteady hydrodynamics occurs at that point at which critical AOA is reached and the flow is no longer attached to the wing. The drag coefficient (C_D) increases whilst the lift coefficient (C_L) decreases, fully stalling the object (*Muijres et al. 2008, Shyy et al. 2009, Yoon et al. 2011, Taira et al. 2009*).

There is a way to postpone stall effects. Either the subject increases the thickness of its leading edge thereby promoting attached flow and thus promoting steady/laminar flow. Or the subject depends on unsteady hydrodynamics for beneficial yet unstable lift enhancement. Leading-Edge Vortex (LEV) formation is such a beneficial yet unstable lift enhancer, LEV mimics an increase in leading edge thickness. By mimicking an increased leading edge thickness, LEVs allow for prolonged and sustained steady hydrodynamics where under conventional hydrodynamics the hydrofoil would experience stall and overall decrease in lift. LEV formation increases the available range of AOA and thereby the available lift for the hydrofoil (*Canfield 2009, Beem et al. 2012, Habib 2012*).

A vortex, created by the LEV, appears on top of the leading edge significantly increases the wings' circulation. The vortex adds its own vorticity to the wings bound vorticity, thereby increasing the wings circulation. Circulation is a part of lift production (4) thus increased circulation results in to increased lift production (*Lehman 2004*, *Canfield 2009*, *Taira & Colonius 2009*, *Shyy et al. 2010*). Unfortunately this lift increase comes with a price, for it is combined with an increase in drag as the AOA increases (*Dickson & Dickinson 2004, Lu et al. 2006, Canfield 2009).* LEV formation is therefore only beneficial up to a certain AOA, at which the increase in lift coefficient has a larger effect on the flipper than the increase in drag coefficient.

A part from studying an increase in lift, to identify LEV formation, the manner in which lift increases over the angle of attack also reveals whether there is an LEV present. Under steady hydrodynamic circumstances, the lift coefficient for an infinite hydrofoil increases linearly with AOA, up to a critical

AOA, at which the lift coefficient decreases instantaneously (*Figure 1*). When the hydrofoil is under unsteady hydrodynamic circumstances, the lift coefficient is significantly increased and critical AOA is delayed. This increases the experienced lift coefficient on the hydrofoil, as well as it's increase in viable (lift producing) angles of attack (*Canfield 2009*). The manner, in which C_L increases over AOA, is a method to determine whether the lift is enhanced by LEVs or not.

So far, LEVs were thought only to be available to insects, who have extremely thin leading edges, their flight can only exist through LEV formation. However, *Muijres et al. 2008*, found that Pallas' long-tongued bats (*Glossophaga soricina*) also use LEVs to increase C_L during flight. This effect was found on bird wings as well (*Canfield 2009*). This recent discovery opened up the possibility for the presence of LEV enhanced flight in other birds, including those with aquatic propulsion.

Usherwood and Ellington (2002) studied the hydrodynamic effects on a revolving insect wing. They concluded that a revolving wing mimics the hydrodynamics of a flapping wing. These revolving wings visualized the same conical Leading-Edge vortex as flapping wings have shown. *Canfield (2009)* also tested LEV formation on bird wings in a revolving system, and saw similar effects, thus agreed with *Usherwood and Ellington's 2002* conclusion. However the LEVs on rotating wings are stable, while those on flapping wings are not.

The LEVs on rotating wings are stable because of the overall pull towards the wing-tip (span-wise flow), forcing a conical LEV shape. In a rotating system LEVs shed near the wing-tip, but are continuously forming at the base of the wing due to this span-wise flow. This flow is not continuously present in flapping wings, as each ending (reaching the bottom of a stroke or the maximum of a stroke) results in a sudden decrease in speed and loss of lift. Once they continue with their stroke, they build up any possible LEV formation until they reach their maximum or minimum state of their stroke after which this LEV breaks away from the wing.

Span-wise flow results in smaller vortex formation at the base of the wing (due to lower velocities). But vortex diameter increases over the span of the wing (as velocity increases, due to increase in distance travelled per time). The vortex is pulled towards the wing-tip, increasing the size of the vortex up until it reaches a critical point (*Usherwood & Ellington 2002a,b, Muijres et al. 2008, Ellenrieder et al. 2008*). At that point, the radius of the vortex has exceeded the chord-length of the wing, falling away from the wing, hence the LEV is unable to attach the oncoming flow to the wing.

A rotating wing mimics the hydrodynamic play of that on a flapping wing, however it does assume continuous performance of the LEVs. It depicts perfect and enhanced flight (*Usherwood & Ellington 2002a, Sane 2003, Canfield 2009, Bandyopadhyay et al. 2012*).

Penguins have large leading edges (*Bannasch 1995*); therefore they potentially rely on a significant amount of attached flow, thus steady hydrodynamics, to produce their lift. However, in order to substantially increase their range of angle of attack and still maintain high lift coefficient, they could rely on LEVs to enhance their propulsive forces as well.

This study focuses on the flippers of the Adélie penguin, and whether the Adélie penguin enhances its underwater flight through the use of unsteady hydrodynamics, LEV formation.

During this project the C_L and angle of attack will be monitored and calculated with a downscaled 3D model of a NACA hydrofoil (NACA 63-018) this hydrofoil resembles the flippers of the *Pygoscelid* penguin group according to *Stamhuis (unpubl).* The model was tested in a rotary system, subjected to varying velocities, and varying angles of attack. DPIV analysis determined whether the penguin relies on steady or unsteady hydrodynamic effects for its underwater flight.

MATERIAL & METHODS

PENGUIN FLIPPER DESIGN

The *Pygoscelid* penguin group contains 3 penguin species: Adélie (*Pygoscelis adeliae*), Chinstrap (*P. antarcticus*) and the Gentoo penguin (*P. papua*). Cross-sections of the flipper of the *Pygoscelid*s, most resemble the NACA 63-018 hydrofoil (*Bannasch 1995*).
The flippers of the Adélie and Chinstrap penguin are most similar to each other. The Gentoo penguin has a slightly smaller chord-length at the upper part of the flipper (*Figure 2*).

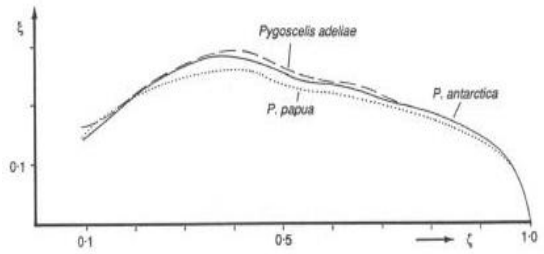

Figure 2. *The outline flipper of the Pygoscelid penguin group. The line consists of the distance between the leading edge of the flipper and the trailing edge of the flipper, the chordlength (given in fractions of flipper length)17.41, 18.28, 21.08 cm, for Adelie, Chinstrap and Gentoo resp. (Bannasch 1994)*

A 3D wing model was made with a 3D printer from light-hardening transparent resin (SLA-epoxy clear 0.1 mm). The model was downscaled, to 13.5 cm, in order to minimize 'wall effects' during the experiments.
Average speeds, single wing area and aspect ratio of the *Pygoscelid* group have been studied (*Table 1*). These observations were used for further experimental set-up.

Flipper length and chord-lengths (*Bannasch 1994*) along with NACA profiles (mostly 63-018), were used to build a downscaled Adélie penguin flipper in Rhinoceros. (64-bit, trial version) (*Appendix I).*
To truly capture the shape of the Adélie penguin flipper a few modifications were made, to the base NACA profiles, starting at the base up to the cross-section of maximum chord-length (*Table 2*). Main reason for this, was to maintain a maximum thickness of 7.2 mm, from base up to the cross-section of maximum chord-length (0 - 52 mm, flipper length). These modifications in NACA profiles (which were all derived from the 63 series) resulted in the use of the profiles: 63-040, 63-038, 63-035, 63-032, 63-024, 63-020 (respectively). This promoted a more natural flipper shape, with increased thickness at the base (reflecting internal bone structure) (*Appendix V*).

FLOW TANK

The flow tank is a cylindrical polyethylene tank, with a 1m diameter and 1.2m in height. It has two glass windows, both used for either flow observation (camera) or visualization (laser) (*Figure 3*).
The two rails on top of the tank act as a mount for the rotary system. The flow tank is filled with fresh water (20°C) up to approx. 1.10m (0.86m^3). The flow tank was built to test flow phenomena on rotating hydro- or aerofoil's in water at higher Reynolds numbers (Re >20,000).
The rotary system revolved the penguin flipper at set motor frequencies (40, 45 and

Table 1. Averages of the Pygoscelid penguin group used during the experiments. (Aspect Ratio= flipper length (in m)^2/single wing area(m^2)). Sources*: Clark & Bemis 1979[1], Baldwin 1988a[2], Culik et al. 1991[3], Amat et al. 1993[4], Culik & Wilson 1994[5], Bannasch 1994[6], Wilson et al. 1996[7], Wilson et al. 2000[8], Sato et al. 2002[9], Sato et al. 2007[10], Ropert-Coudert et al. 2007[11], Sato et al. 2010[12], Bandyopadhyay et al. 2012, Wilson & Grémillet 1996[13]. Dam et al 2002.*

Species	***Single wing area (m^2)***	***Average swimming speed (m/s)***	***Flipper length (m)***	***AR***
Adélie ***Pygoscelis adeliae***	0.0072[12]	2.1 – 2.4[3,5,9,12]	0.17[6,12]	8.42[6]
Gentoo ***Pygoscelis papua***	0.0098[12]	1.7 - 2.3[3,7,10,12]	0.21[6,12]	9.07[6]
Chinstrap ***Pygoscelis antarctica***	0.0078[12]	2.3 - 2.5[3,10,12]	0.18[6,12]	8.57[6]

50 Hz, which gives; 2.90, 3.26 & 3.63 m/s as base rotation speeds. The flipper set at angles of attack ranging from 0°C to 32.5°C with a step size of 2.5 degrees

SET-UP EXPERIMENTS

As mentioned, the model was exposed to warmer and fresh water during the experiments (20°C, salinity 1.5%). The Adélie penguins, in their natural habitats, are exposed to cold seawater (4°C, salinity 34.7%). Calculating the Reynolds number of the model revealed the real-life swimming velocity of the Adélie penguin, at which it was compared with studied swimming velocity. In this manner, the experiment would reflect true Adélie penguin swimming behavior.

Reynolds number is a dimensionless number that reflects the hydrodynamic state of the object. It is determined by, kinematic viscosity (which, in turn, is affected by temperature and density), chord and velocity, as follows:

$$Re = \frac{vc}{K_v} \qquad (1)$$

Kinematic viscosity of both natural and tank circumstances are 1.626×10^{-6} & 1.004×10^{-6} resp. The maximum chord length of the Adélie and model: 51.5 mm and 40 mm resp. In order to keep the Reynolds numbers identical, base rotation velocity of the rotary set-up was increased (the model needed to be rotated faster than the free-swimming penguin would normally reach) (*Table 2*).

DIGITAL PARTICLE IMAGE VELOCIMETRY

DPIV, laser technique, revealed whether the flipper of the penguin experiences steady or unsteady hydrodynamic effects. The additional aspect to using this technique, instead of qualitative analysis with dye, gives the opportunity to quantify the Lift coefficient (C_L).

Small (57 microns in diameter) polyamide particles were added to the flow tank. Their density is higher than that of fresh water (polyamide: 1.016 g/ccm) and therefore, according to *Stokes Law*, will sink to the bottom at approx. 0.25 microns/sec (2). This effect is minimal, and was therefore not taken into account in analysis. Dynamic viscosity of water at 20°C is approx. $1.0 * 10^{-3}$ $N(s/m^2)$

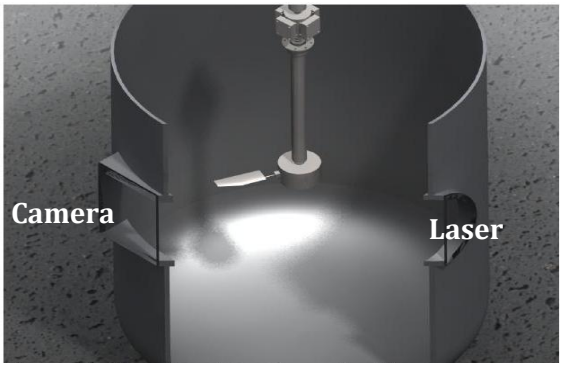

Figure 3. Inside view of the flow tank, built by *P. Canfield, E.J. Stamhuis & D.E. Worst*. A rotary device in the middle of the tank rotates the wing at controlled frequencies (Source: *Canfield 2009*). Laser and camera are set on 90^0 angle apart. Both camera and laser set at 13.5 cm away from glass.

$$V_s = \frac{2}{9}\frac{(\rho_p - \rho_f)}{\mu} g R^2 \qquad (2)$$

The particles were illuminated by a vertical green laser sheet (5W) via the round window (*Figure 3*). The laser sheet was set perpendicular to the camera. This laser set up allowed for flow movement capture above and below the flipper, necessary for entire flipper flow analysis. Unfortunately, the model was not entirely transparent and blocked much light once set at higher AOA.

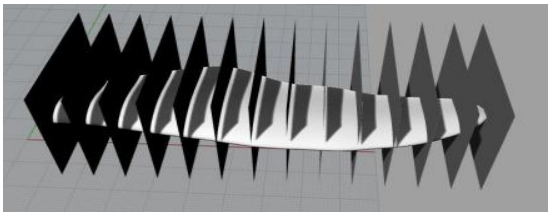

Figure 4. Schematic view from above, shows where the laser was set to create cross-sections of the wing for hydrodynamic analysis in Pivlab (Image from Rhinoceros). First point at 5mm, each next cross-section 10mm removed from the other (except for the last cross-section, set at 134mm from base). See Appendix IX for real-life top view of the flipper with laser.

Table 2. Length displays distance from base of the flipper at which the cross-section was measured. Chord-length displays the length of the chord at that cross-section. Three columns for velocity depict the rotation velocity per cross-section at a certain base rotation velocity (with mechanical rotation force set to 40, 45 & 50Hz). Distance on flipper equals distance from base (b).

Cross-section #	***Distance on flipper/b* (m)**	***Chord-length* (m)**	***Velocity* (m/s) *(mech. 40Hz)***	***Velocity* (m/s) *(mech. 45Hz)***	***Velocity* (m/s) *(mech. 50Hz)***
1	0.005	0.019	1.30	1.46	1.63
2	0.015	0.023	1.54	1.74	1.94
3	0.025	0.029	1.79	2.02	2.24
4	0.035	0.034	2.03	2.29	2.55
5	0.045	0.038	2.28	2.57	2.86
6	0.055	0.040	2.52	2.84	3.16
7	0.065	0.037	2.77	3.12	3.47
8	0.075	0.034	3.01	3.40	3.78
9	0.085	0.033	3.26	3.67	4.09
10	0.095	0.030	3.50	3.95	4.39
11	0.105	0.027	3.75	4.22	4.70
12	0.115	0.023	3.99	4.50	5.01
13	0.125	0.018	4.24	4.78	5.32

Both the camera and Laser were set to an downward angle of 11.7˚C to compensate the upward angle of the flipper attachment (the flipper had an upward angle which was 11.7˚C at the wing-tip).

The camera filmed the illuminated particles and provided raw image data of particle movement. The data were converted to relative particle displacement and recalculated to a vector through digital PIV-analysis using PIVlab© (*Thielicke, W. & Stamhuis, E. J. (2014): PIVlab - Time-Resolved Digital Particle Image Velocimetry Tool for MATLAB*).
Camera was set to 600 fps and exposure time was 1664. Camera sensitivity set to maximize the amount of light entering the lens. Laser was set to maximum power.
The flow around the wing was mapped in fourteen equidistant planes (*Figure 4)*. In all of these planes the flipper has a specific chord length, and specific velocity (*Table 2.).*

JAVAFOIL

We use Javafoil in order to compare our results with that of a simulated infintite (2D) wing. In which case we can compare produced lift of our flipper with estimated and simulated values for our flipper in 2D.
The main hydrofoil used to create the 3D penguin flipper is NACA 63-018 and therefore we assume the JAVAfoil analysis of the NACA 63-018 to be a good estimate of proposed lift production.
We added in our three base velocities (40,45 and 50 Hz – for which we averaged the values over the entire flipper) and combined that with our tested angles of attack.

ANALYSIS

Images from the Real-time Image Recorder were analyzed with PIVlab©, a DPIV-tool running within Matlab. In PIVlab a square (interrogation area) from one image (a) is compared with an interrogation area in the following image (b). 'a' has a specific pattern of particles and must be present in 'b', thus the program tries to match 'a' with 'b' (twisting and turning it) to come up with a distance travelled factor (aka a vector). These calculated vectors show the flow phenomena and translate them to vortices, if present.

In PIVlab, circulation is measured with the tangent velocity. The tangent velocity is derived from the distance from core and angular verlocity (vorticity, ω) (3, *Milne-Thompson 1966*). Tangent velocity analysis was performed in two ways. Through polyline analysis (*Figure 5*), drew the best fitting line around the cross-section, or allow PIVlab to draw circle series around the cross-section. In both cases, the maximum circulation was used for further calculations.

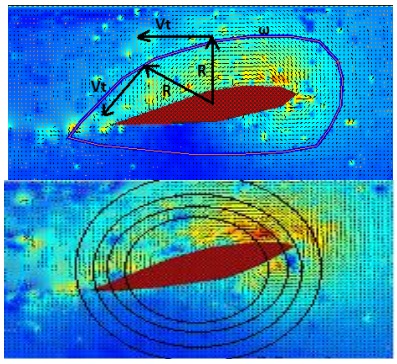

Figure 5. Polyline Circulation analysis in PIVlab (top), blue line indicates the drawn polyline of which PIVlab calculated the tangent velocity, the integral of the tangential velocity provides us with a circulation accountable for one cross-section at set velocity and angle of attack. Frame of cross-section #6 at 50 Hz & AOA 12.5°C. Circle Circulation analysis in Pivlab (bottom). For the Circle analysis multiple circles were drawn into the the frame (up to 30 circles). Each circle has a circulation value (calculated as the polyline circulation analysis).The hydrofoil in this case has an elongated shape thus the circle circulation method was not adequate for our analysis.

$$V_T = r\omega \quad (3)$$

$$\Gamma = \oint_c \overrightarrow{v_T}\, d\vec{v} \quad (4)$$

$$L = pv\Gamma b \quad (5)$$

$$C_L = \sum 0.5pv^2AL \quad (6)$$

Circulation (4) is calculated per cross-section (with the Polyline circulation method provided in Pivlab, *Figure 5*). Circulation is the integral of the tangential velocity around the loop.

With this cross-section circulation, following lift is calculated (blade element approach*, Stamhuis et al. 2011*) (5). Each equidistant plate has a corresponding velocity which depends on the base rotation velocity (*Table 2*). Each plate has b distance from the base of the flipper, multiply it by b reveals the lift over a equidistant plate of b length. We calculated Lift per plate measured and thus b symbolizes distance between two measured plates (starting at 0.5 cm, 1.5 cm, 2.5 cm etc.). All these factors were necessary to calculate the dimensionless number C_L (*Figure 7*). Thus I only summed after completing the lift coefficient formula (6) per cross-section/equidistant plate. This sum resulted in the lift force acting over a flipper at one single base speed at one single angle of attack.

LIST OF SYMBOLS

A	Single wing area
α	Geometric Angle of Attack
AR	Aspect Ratio
b_i	Wing-span (i: location on the flipper)
c	Wing chord-length
C_D	Drag coefficient
C_L	Lift Coefficient
g	Gravitational acceleration
K_v	Kinematic viscosity
L	Lift
ρ	Density of water
ρ_f	Density of water (20°C)
ρ_p	Particle density
R	Particle Radius
r	Distance from wing center
Re	Reynolds number
U	Velocity of cross-section
v	Velocity
V_s	Settling velocity (derived from Stokes Law)
v_t	Tangent velocity
ω	Vorticity (angular velocity)
μ	Dynamic viscosity of water (20°C)
Γ	Circulation

RESULTS

The three tested mechanical rotation forces (at 40, 45 and 50 Hz) show a significant difference in circulation (t-test two sided paired, $p<<0.05$).

There is no significant difference between polyline or circle circulation analysis. Because the polyline method allowed for actual shape following of the wing, we decided to use only polyline circulation results for further calculations.

First we added all circulations found per angle of attack together (*Figure 6*). This signifies the effect chord-length has on the circulation of the flipper. Although chord-length shows a significant effect on circulation, b (and thus rotation velocity) shows an even greater effect on circulation.

NACA 63-018 JAVAfoil 2D analysis shows the lift to reach maximum force at approximately 17.5°C, after which the lift drops significantly, negatively correlated with the increasing angle of attack.

NACA 63-018 hydrofoil 3D Adélie flipper still shows an increase in lift at AOA 15°C, and has not yet reached its maximum lift at 17.5°C either (*Figure 7*). A significant decline in lift is measured beyond 20°C.

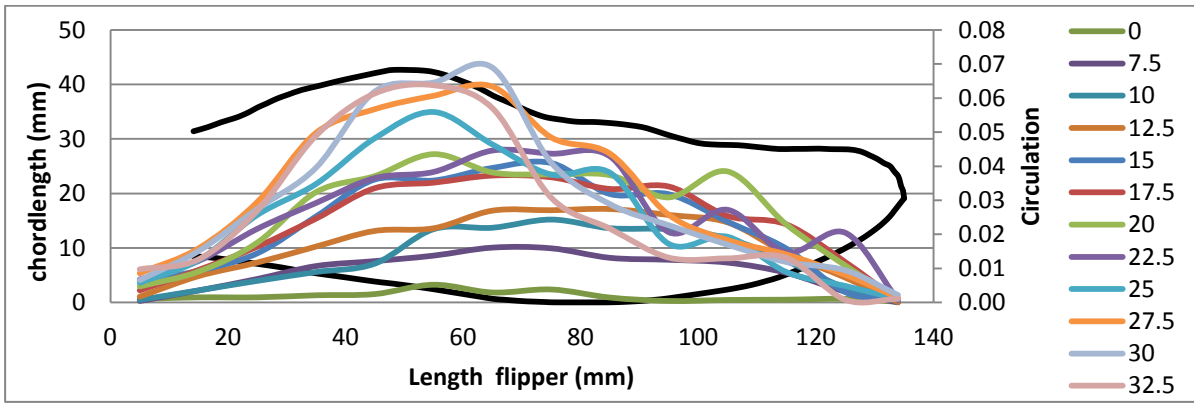

Figure 6. Circulation and distance of length and chord-length on the flipper at different angles of attack (from 0 to 32.5 °C). Black line depicts outline of the 3D printed Adelie penguin flipper in mm. Maximum circulation found at maximum chord-length (c=0.04m). This figure shows how the chord-length affects Γ, an increase in chord-length, leads to an increase in Γ , with the opposite being true as well. However, chordlength increases and decreases over length of the flipper, velocity of the wing only increases as it moves from base to the wing-tip. Velocity should have an affect on Γ, however it is masked by the effect caused by the chord-length.

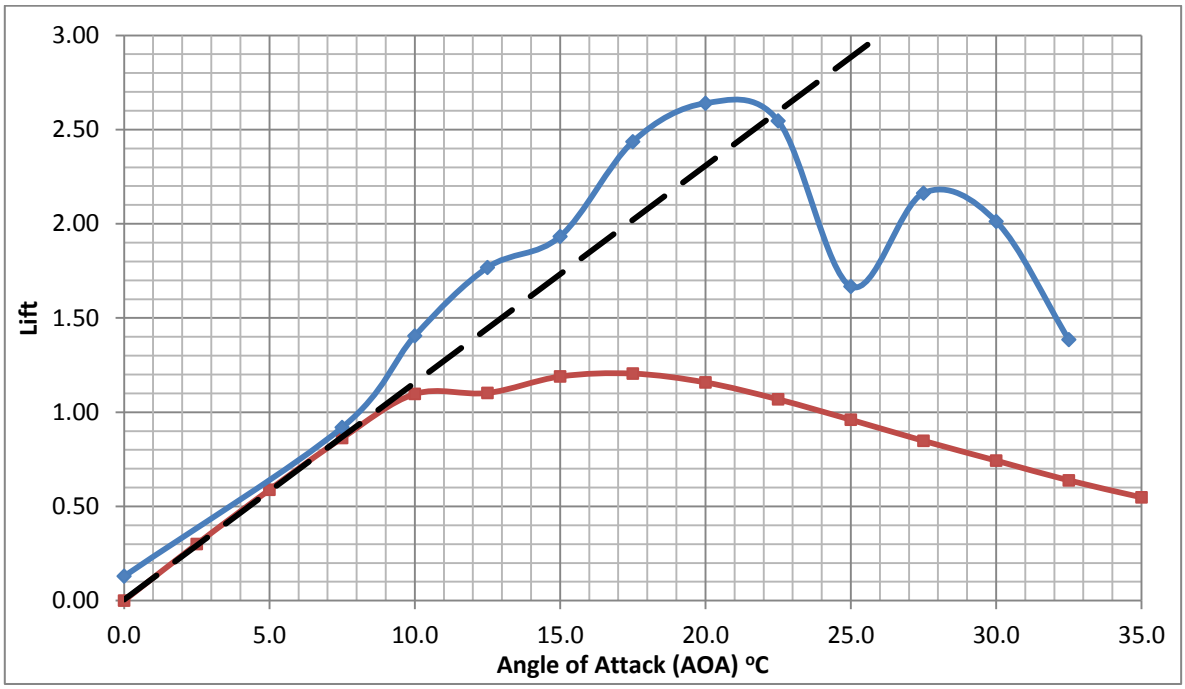

Figure 7. The average Lift coefficient set to Angle of attack. Black striped line shows the linear increase of Lift according to Javafoil (assumes an infinite wing). The red line shows predicted lift coefficient of the NACA 63-018 profile according to Javafoil (assumes an infinite wing). The blue line shows the finite (3D) models result. Peak Lift coefficient is found at 20°C and quickly declines thereafter. The sudden decrease at 25°C is present in all three base speeds, for now it remains uncertain what caused this effect. The increase in Lift of the Adélie model occurs linear up to 7.5°C after which the it increases at even greater speed and continues to do so up until reaching 20°C. Overall, maximum (averaged) Lift coefficient reached is 2.65 as opposed to 1.2 as expected (2D Javafoil analysis). Maximum lift coefficient reached by the highest base velocity (50 Hz, 3.63 m/s) is 3.64 (Appendix VIII).

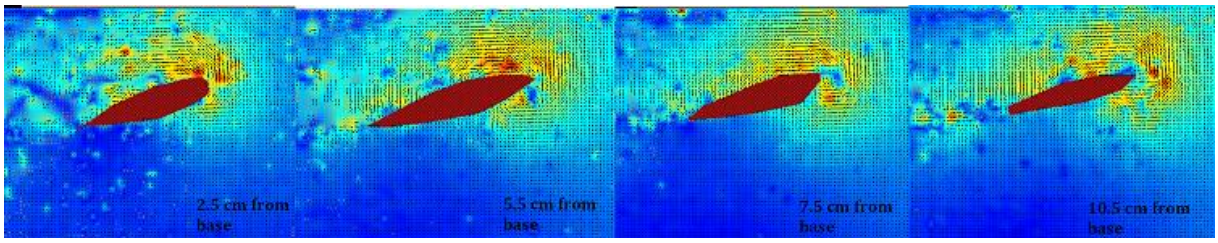

Figure 8. PIVlab analysis of the flipper at $b_{2.5}$, $b_{5.5}$, $b_{7.5}$ and $b_{10.5}$ for AOA = 17.5° at base frequency of 40 Hz (average velocity 2.90 m/s). Blue to red signifies the intensity of the magnitude velocity surrounding the flipper, with the highest magnitude velocities colored red. In $b_{2.5}$ the highest velocity magnitudes appear to be surrounding and covering the leading edge of the flipper. At $b_{5.5}$ there is a noticeable gap near the underside of the leading edge, in this area there is a low magnitude velocity. Although in $b_{5.5}$ there is also a larger point of increased velocity magnitude on top of the leading edge. The 'dead'-zone first visible at $b_{5.5.}$ moves upwards and ends up on top of the flipper as the distance between base and cross-section increases. In $b_{7.5}$ the increased magnitude velocity point has disappeared and results in overall increase over the entire top-side of the flipper. In $b_{10.5}$ there are now two 'dead'-zones both on top of the flipper and one on top of the leading edge. In $b_{10.5}$ there are two points of increased velocity magnitude, one on the center of the top side of the flipper, the other in front of the leading edge (in front of the 'dead'-zone).

DISCUSSION

There was no significant difference between the polyline and circle method of circulation analysis in Pivlab. However, because of the shape of the hydrofoil, I opted to use the polyline method for it contoured the shape of the hydrofoil more precisely. The circles used for circulation analysis could give inaccurate circulation readings, although, our analysis shows that both the polyline and polycircle method provide similar information.

The delay in lift decay in our model and thus the delay of critical angle of attack in a model (compared to expected 2D Javafoil calculations) depicts a possible scenario for LEV formation. Characteristics of LEV formation are; larger than linear increase in lift to angle of attack ratio, and delayed critical angle of attack (*Stamhuis et al. 2011*) Up to an AOA of 7.5°C, the increase of C_L is linear in our model, however past that point, the increase of C_L is even higher (*Figure 7*), $C_{L\alpha(<7.5)}$ = 0.12 and $C_{L\alpha(>7.5)}$ = 0.14 (with maximum value of 0.21 C_L/α). Compared to the 2D analysis of the NACA 63-018 hydrofoil (JAVAfoil, with 0.11 C_L/α) our found continuous growth of C_L supersedes anything expected. It is only after an angle of 20°C that there is steep decrease in C_L (*Figure 7*).

It is interesting that the three chosen base velocities (they are n.s., *Figure 7* & *Appendix VIII*) all show a sudden decline in lift coefficient at 25°C. What the exact reason is for this phenomenon is yet to be determined. Perhaps at this point the drag coefficient has increased so substantially that it disintegrates the positive lift force provided by the (probable) LEV formation. Although if it were only a sudden increase in drag coefficient, we would expect this effect to continue throughout the increasing angles of attack. However, both *Figure 6* and *Appendix VIII* reveal a second, although smaller, lift coefficient peak at 27.5 °C or 30 °C (for machine rotation 'velocity' 40, 45 and separate peak for 50 Hz respectively). Although all tested base velocities show similar patterns, their results are significantly different from each other. With an apparent increased effect in Lift enhancement over AOA at the highest base velocity (50Hz). More data is necessary to be able to answer what causes this strong increase, for our current data-set relies on n=1 per base velocity.

Figure 8 shows 4 cross-sections with increasing distances from the base at an equal AOA of 17.5°C. This is the AOA just before the flipper reaches maximum lift coefficient (found at 20 °C). In this case the circulation of the wing was still increasing tremendously as AOA increased. The red part indicates the highest velocity magnitude, thus arguably in this case, the centre of the leading edge vortex. This vortex is clearly present in the first figure

just 2.5 cm removed from the base. There are multiple red spots in this cross-section, although one truly stands out from the rest, thus arguably the centre of the vortex. There is also a clear increase of speed around the leading edge of the wing. With an increase in speed on the top side of the wing. So far there is very little shedding at the trailing end.
The 2nd cross-section shows an even larger epicenter of the vortex. The overall velocity magnitude has also increased on the topside of the wing. This increase in velocity is present over the entire top end and leading edge of the flipper, as if the water is cocooning the flipper.

Both the 3rd and 4th cross-section show a 'dead' space right in front if the leading edge, it appears that surrounding water is pulled over the flipper. This dead space is already present in the 2nd cross-section, although at the bottom of the wing, and as we continue towards the wingtip we see this 'dead space' move towards the center and enveloping the entire leading edge in the 4th cross-section. It seems that this dead space mimics an increase in leading edge thickness, this might enable the flipper to continue grow in lift coefficient, even although conventional hydrodynamics would not allow this to happen.
The 4th cross-section is near the end of the flipper and there are signs of a tip-vortex present. There are small high magnitude velocity circles shredding from the flipper and ending behind it. There are also two 'dead'-zones present, one in front of the leading edge and the other center of the topside of the flipper. The 'dead'-zone in front of the flipper is very interesting, for there appears to be a vortex (point of increased magnitude velocity) right in front of that 'dead'-zone. Does this 'dead'-zone act as an elongation of the leading edge? What the exact reason is for its presence, and thus its effect, has yet to be determined.

Continuous analysis far beyond the angle of attack of 32.5°C was restricted due to our experimental set-up. Increasing the angle of attack up to 35°C resulted in unwanted effects (i.e. shaking) of the rotary system. Our system was incapable of rotating the flipper at such high AOA at base velocities above 30Hz. Thus we excluded any higher angles of attack in our analysis.
It seems that at higher angles of attack, the drag created by the flipper, was too large for the rotary system to maintain. It is therefore, arguably, impossible for the Adélie penguin to keep its flippers at such high angles of attack during underwater flight. The drag alone would, most likely, stall the penguin mid flight. This observation is confirmed by our lift calculations, as there is a drop in lift after 27.5 °C, at our highest tested AOA (32.5 °C) lift had dropped to 1.35 (from 2 at 30 °C).

It is interesting that the wings' velocities do not have a clear effect on circulation (*Appendix VII*). It appears that when c increases, circulation increases (*Figure* 6) and vice versa. However, considering that velocity increases over the wing, creating even more unsteady effects as it increases (the oncoming flow will need to rapidly bend along the hydrofoil as the velocity increases, and as AOA increases, this will prove to become even more difficult.) it can be argued that this increase in velocity over the wing (and not the decrease in c, *Appendix VI*) causes the circulation to drop. Unfortunately, this can not be ruled out for this data set, further analysis will be necessary.

According to *Lovvorn et al. 2001*, feathers on the fuselage had a greater effect on drag than the shape of the penguin fuselage. There was a 2-6 fold increase in drag coefficient found in frozen penguin fuselage specimens. And *Davenport et al. 2011* reported that the feathers of emperor penguins, and their release of air whilst diving, decreased C_D significantly. If we had added the presence of feathers to the mixture, maximum lift coefficient could even be higher. Our results are, however, already very high, this is due to our set-up. According to *Usherwood & Ellington 2002*, this set-up mimics similar hydrodynamic effects as a flapping wing. Although it might be similar, testing only rotational motion, denies the presence of translational motion and its impact on the hydrodynamics around the flipper. It is probable that found

Lift coefficients, which are extremely high, are overestimations of the actual situation. Nonetheless, the data shows a clear non-linear increase between an angle of attack of 15 ^{o}C and 20^{o}C which can not be explained by conventional steady hydrodynamics.

The manner in which maximum lift is achieved and then drops differs strongly between estimated 2D JAVAfoil analysis and our lift results (*Figure 7*). With JAVAfoil analysis lift seems to slowly reach its maximum lift and then steadily drops as the angle of attack increases. This signifies a gradual increase in drag which results in the loss of overall lift. Our analysis, however, shows a second peak after the maximum lift as well as two very rapid lift decline moments. By just comparing the manner in which lift disintegrates, we can conclude that our lift behaves much more unsteady than the expected JAVAfoil lift does.

Our set-up might reveal lift-values under the most 'optimal' circumstances, but there is still an increase in lift, when compared to 2D analysis. Our experiment has provided us the basics of hydrodynamic play on a rotating penguin flipper. Research that follows should continue to build towards more realistic movement of the flipper (flapping flight) in order to establish the magnitude in which the lift of the Adélie penguin is enhanced. Although this would indeed give us more accurate readings on actual lift enhancement/production of the Adélie penguin flipper, the use of both translational and translatory movement involved in flapping flight, complicates the experiment. This adds another dimension with build up and shedding of vortices and thus lift. It would require continuous registration of the flipper during each step of the stroke. In which case, our experiment provides details in lift in the most optimal position. It allows us to 'stabilize' the unsteady hydrodynamics that are at play on the Adélie penguin flipper.

CONCLUSION

Do steady or unsteady hydrodynamic effects determine hydrodynamic flow over the penguin flipper?

Our data concludes a significant increase in lift and delay of critical angle of attack. PIVlab analysis depicts high velocity magnitudes on top of the flipper, which supports the hypothesis of an LEV enhancing the Adélie penguins' lift.

Because the lift is significantly increased, as well as delayed stall effects, we conclude that unsteady hydrodynamic effects determine hydrodynamic flow over the penguin flipper.

However, the rotary system has an increased stabilizing effect of LEV formation and our lift values are larger than expected. Our results are assuming an ideal situation, and further investigation with actual flapping mechanics is necessary to establish how much the formation of LEVs increase the Adélies' lift.

REFERENCES

1. ***Baldwin J.*** *(1988) Predicting the swimming and diving behaviour of penguins from muscle biochemistry. Hydrobiologica Vol. 165. pp. 255-261.*
2. ***Bandyopadhyay P.R., Beal D.N., Hrubes J.D., Mangalam A.*** *(2012) Relationship of roll and pitch oscillations in a fin flapping at transitional to high Reynolds numbers. J. Fluid Mech. Vol. 702. pp. 298-331.*
3. ***Bannasch R., Wilson R.P., Culik B.*** *(1994) Hydrodynamic aspects of design and attachment of a back-mounted device in penguins. J. exp. Biol. Vol. 194. pp. 83-96.*
4. ***Bannasch R.*** *(1994) Functional anatomy of the 'flight' apparatus in penguins. Maddock L., Bone Q., Rayner J.M.V. (ed.). Mechanics and Physiology of Animal swimming. Cambridge University Press. Pp. 163-192.*
5. ***Bannasch R.*** *(1995) Hydrodynamics of penguins – an experimental approach. In The Penguins: Ecology and Management (ed. P. Dann. I. Norman and P. Reily). pp. 141-176. Chipping Norton: Surrey Beatty & Sons.*
6. ***Bannasch R.*** *(1997) Experimental studies on the Boundary Layer development in Penguins: mechanisms of turbulence control and their applicability to Engineering.*
7. ***Beem H.R., Rival D.E., Triantafyllou M.S.*** *(2012) On the stabilization of leading-edge vortices with spanwise flow. Exp. Fluids vol: 52, pp:551-517.*
8. ***Bilo D.. Nachtigall W.*** *(1980) A simple method to determine drag coefficients in aquatic animals. J. exp. Biol. Vol. 87. pp. 357-359.*
9. ***Butler P.J.*** *(2000) Energetic Costs of Surface Swimming and Diving of Birds. Physiological and Biochemical Zoology Vol. 73. No. 6. pp. 699–705.*
10. ***Canfield P.*** *(2009) Aerodynamics of revolving wing models. Msc-thesis University of Groningen.*
11. ***Clark B.D.. Bemis W.*** *(1979) Kinematics of swimming of penguins at the Detroit Zoo. J. Zool. Lond. Vol. 188. pp. 411-428*
12. ***Culik B.M.. Wilson R.P.. Dannfeld R.. Adelung D.. Spairani H.J., Coria N.R.C*** *(1991) Pygoscelid penguins in a swim canal. Polar Biol. Vol. 11. pp. 277-282*
13. ***Culik B.M., Wilson R.P.*** *(1991) Swimming energetic and performance of instrumented Adélie penguins (Pygoscelis adeliae). J. Exp. Biol. Vol 158, pp. 355-368.*
14. ***Culik B.M., Wilson R.P.*** *(1994) Underwater swimming at low energetic cost by Pygoscelid penguins. J. Exp. Biol. Vol. 197. pp. 65-78*
15. ***Dam R.P. van. Ponganis P.J., Ponganis K.V.. Levenson D.H., Marshall G.*** *(2002) Stroke frequencies of emperor penguins diving under sea ice. The Journal of Experimental Biology 205. 3769-3774.*
16. ***Davenport J., Hughes R.N., Shorten M., Larsen P.S.*** *(2011) Drag reduction by air release promotes fast ascent in jumping emperor penguins – a novel hypothesis. Mar. Ecol. Prog. Ser. Vol. 430. pp. 171-182*
17. ***Dickson W.B. and Dickinson M.H.*** *(2004) The effect of advance ratio on the aerodynamics of revolving wings. The Journal of experimental Biology. Vol. 207. pp. 4269 – 4281.*
18. ***Ellenrieder von, K.D. Parker K., Soria J.*** *(2008) Fluid mechanics of flapping wings. Experimental and Fluid Science. Vol. 32, pp. 1578-1589.*
19. ***Ellington. C.*** *(2006) Insects versus birds: the great divide. 44th AIAA Aerospace Sciences Meeting and Exhibit. 6. 1*
20. ***Fish. F.E.*** *(1993) Influence of hydrodynamic design and propulsive mode on mammalian swimming energetics. Australian Journal of Zoology Vol. 42. pp. 79–101.*
21. ***Fish F.E.*** *(1998) Imaginitive solutions by marine organisms for drag reduction. Symposium Westchester University.*
22. ***Fish F.E.*** *(2000) Biomechanics and energetics in aquatic and semiaquatic mammals: platypus to whale. Physiol Biochem Zool. Vol. 73, pp. 683–698.*
23. ***Fish F.E.. Howle L.E.. Murray M.M.*** *(2008) Hydrodynamic flow control in marine mammals. Integrative and Comparative Biology. Vol. 48. No. 6. pp. 788–800.*
24. ***Habib M.*** *(2010) The structural mechanics and evolution of aquaflying birds. Biological Journal of the Linnean Society. Vol. 99. pp. 687 – 698.*
25. ***Ho S., Nassef H., Pornsinsirirak N., Tai Yu-C., Ho C.-M.*** *(2003) Unsteady aerodynamic and flow control for flapping wing flyers. Progression in Aerospace science. Vol. 39, pp. 635-681.*
26. ***Hui C.A.*** *(1988a) Penguin swimming I. Hydrodynamics. Physiological Zoology. Vol. 61. No. 4. pp. 333-343.*
27. ***Hui C.A.*** *(1988b) Penguin swimming II. Energetic and Behavior. Physiological Zoology. Vol. 61. No. 4. pp. 344-350.*
28. ***Ito S., Harada M.*** *(2003) Diving simulation concerning Adélie penguin. JSME International Journal Series C. Vol. 46. No. 4. pp. 1363 – 1367.*
29. ***Jackson. P.S., Locke. N. & Brown. P.*** *(1992) The hydrodynamics of paddle propulsion. Australasian Fluid Mechanics Conference Vol. 11. pp. 1197–1200.*
30. ***Johansson L.C., Aldrin B.S.W.*** *(2002) Kinematics of diving Atlantic puffins (Fratercula artica L.): evidence for an active upstroke. Journal of Experimental Biology Vol. 205. pp. 371–378.*
31. ***Kikker A.*** *(2011) - Influence of surface structures on fluiddynamics using the example of penguin wings (Pygoscelis). Bsc-thesis University of Bremen.*
32. ***Lehmann F.*** *(2004) The mechanisms of lift enhancement in insect flight. Naturwissenschaften. Vol. 91. No. 3. pp. 101-122.*
33. ***Louw G.J.*** *(1992) Functional anatomy of the penguin flipper. JI S. Afr.vet.Ass. Vol. 63. No. 3. pp. 113-120.*
34. ***Lovvorn J.R.*** *(2001) Upstroke Thrust. Drag Effects. and Stroke-glide Cycles in Wing-propelled Swimming by Birds. Amer. Zool. Vol. 41. pp. 154–165.*

35. ***Lovvorn J.R., Liggins G.A., Borstad M.H., Calisal S.M., Mikkelsen J.*** *(2001) Hyrodynamic drag of diving birds: effect of body size. body shape and feathers at steady speeds. The Journal of Experimental Biology Vol. 204. pp. 1547–1557.*
36. ***Lovvorn J.R., Liggins G.A.*** *(2002) Interactions of body shape. body size and stroke-acceleration patterns in costs of underwater swimming by birds. Functional Ecology Vol. 16. pp. 106–112.*
37. ***Lu Y., Shen G.X., Lai G.J.*** *(2006) Dual leading-edge vortices on flapping wings. The Journal of Experimental Biology. Vol. 209. pp. 5005 – 5016*
38. ***Mill G. K., Baldwin J.*** *(1983) Biomechanical correlates of swimming and diving behavior in the little penguin. Eudyptula minor. Physiol. Zool. Vol. 56. pp. 242-254.*
39. ***Milne-Thompson L.M.*** *(1966) Theoretical Aerodynamics. Dover publications inc. New York.*
40. ***Muijres F.T., Johansson L.C., Barfield R., Wolf M., Spedding G.R., Hedenström A.*** *(2008) Leading-Edge Vortex Improves Lift in Slow-Flying Bats. Science. Vol. 319. pp. 1250 – 1253.*
41. ***Pennycuick. C.J.*** *(1996). Wingbeat frequency of birds in steady cruising flight: new data and improved predictors. J. Exp. Biol. Vol. 199. pp. 1613-1618*
42. ***Pinebrook W.E., Dalton C.*** *(1982) Drag minimization on a body of revolution through evolution. Computer methods in applied mechanics and engineering Vol. 39. pp. 179-197.*
43. ***Rozhdestvensky K.V., Ryzhov V.A.*** *(2003) Aerodynamics of flapping-wing propulsors. Progress in Aerospace Sciences. Vol. 39. pp. 585-633.*
44. ***Ropert-Coudert Y., Kato A., Baudat J., Bost C-A., Le Maho Y., Naito Y.*** *(2001) Feeding strategies of free-ranging Adélie penguins Pygoscelis adeliae analysed by multiple data recording. Polar Biology Vol. 24, Issue 6, pp. 460-466.*
45. ***Sane S.P., Dickinson M.H.*** *(2001) The control of flight force by a flapping wing: lift and drag production. The Journal of Experimental Biology 204. 2607-2626.*
46. ***Sane S.P.*** *(2003) The aerodynamics of insect flight. The Journal of Experimental biology. Vol. 206. pp. 4191-4208.*
47. ***Shyy W., Trizila P., Kang C., Aono H.*** *(2009) Can tip vortices enhance lift of a flapping wing? AIAA Journal. Vol. 47. No. 2. pp. 289 – 293.*
48. ***Stamhuis, E. J., Thielicke, W., Ros, I., & Videler, J. J.*** *(2011). Unsteady aerodynamics essential during low speed flapping flight in bird. submitted for publication.*
49. ***Timmer W.A.*** *(2009) An overview of NACA 6-digit airfoil series characteristics with reference to airfoils for large wind turbine blades. 47th AIAA Aerospace Sciences Meeting Including The New Horizons Forum and Aerospace Exposition 5 - 8 January 2009, Orlando, Florida. AIAA 268, pp. 1-13.*
50. ***Trizila P.C.*** *(2011) Aerodynamics of Low Reynolds number. rigid flapping wing under hover and free-stream conditions.*
51. ***Usherwood J.R., Ellington C.P.*** *(2002a) The Aerodynamics of revolving wings. I. Model hawkmoth wings. The Journal of Experimental Biology. Vol. 205. pp. 1547-1564.*
52. ***Usherwood J.R., Ellington C.P.*** *(2002b) The Aerodynamics of revolving wings II. Propeller force coefficients from mayfly to quail. The Journal of experimental biology. Vol. 205. pp. 1565-1576.*
53. ***Videler J.J., Stamhuis E.J. & Povel G.D.E.*** *(2004) Leading-Edge Vortex Lifts Swifts. Science. Vol. 306. pp. 1960-1962.*
54. ***Walker J.A., Westneat M.W.*** *(2000) Mechanical performance of aquatic rowing and flying. Biological Sciences. Vol. 267. No. 1455. pp. 1875-1881.*
55. ***Watanabe Y.Y., Takahashi A.****(2013) Linking animal-borne video to accelerometers reveals prey capture variability. PNAS Vol.110 (6) pp. 2199-2204.*
56. ***Watanuki Y., Wanless S., Harris M., Lovvorn J.R., Miyazaki M., Tanaka H., Sato K.*** *(2006) Swim speeds and stroke patterns in wing-propelled divers: a comparison among alcids and a penguin. The Journal of Experimental Biology Vol. 209. pp. 1217-1230.*
57. ***Weihs D. & Webb P.W.*** *(1983) Optimization of locomotion. Fish Biomechanics (eds Webb P.W. & Weihs D.) pp. 339–371.*
58. ***Wilson R.P., Hustler K., Ryan P.G., Burger A.E., Noldeke E.C.*** *(1992) Diving birds in cold water: do Archimedes and Boyle determine energetic costs? Am. Nat. Vol. 140. pp. 179–200.*
59. ***Wilson R.P. & Liebsch N.*** *(2002) Up-beat motion in swinging limbs: new insights into assessing movement in free-living aquatic vertebrates. Marine Biology Vol. 142. pp. 537-547.*
60. ***Wilson R.P., Shepard E.L.C., Laich A.G., Frere E., Quintana F.*** *(2010) Pedaling downhill and freewheeling up; a penguin perspective on foraging. Aquatic Biology. Vol. 8. pp. 193-202.*
61. ***Yoon H.S., Hung P.A., Jung J.H., Kim M.C****. (2011) Effect of the wavy leading edge on hydrodynamic characteristics for flow around low aspect ratio wing. Computer & Fluids. Vol. 49. pp. 276-289*

APPENDIX

Appendix I NACA 63-018 Hydrofoil Profile.

1.000	0.000
0.992	0.000
0.980	0.001
0.963	0.002
0.941	0.004
0.915	0.008
0.885	0.012
0.852	0.018
0.814	0.024
0.774	0.032
0.731	0.040
0.686	0.049
0.639	0.058
0.591	0.066
0.541	0.074
0.491	0.081
0.440	0.086
0.390	0.089
0.341	0.090
0.293	0.089
0.247	0.086
0.204	0.081
0.163	0.075
0.126	0.067
0.093	0.059
0.064	0.049
0.040	0.039
0.021	0.029
0.008	0.018
0.001	0.007
0.000	0.000
0.001	-0.007
0.008	-0.018
0.021	-0.029
0.040	-0.039
0.064	-0.049
0.093	-0.059
0.126	-0.067
0.163	-0.075
0.204	-0.081
0.247	-0.086
0.293	-0.089
0.341	-0.090
0.390	-0.089
0.440	-0.086
0.491	-0.081
0.541	-0.074
0.591	-0.066
0.639	-0.058
0.686	-0.049
0.731	-0.040
0.774	-0.032
0.814	-0.024
0.852	-0.018
0.885	-0.012
0.915	-0.008
0.941	-0.004
0.963	-0.002
0.980	-0.001
0.992	0.000
1.000	0.000

Appendix II Adélie penguin flipper measurements (x.y) from Bannasch (1994) graph. The x.y-coordinates are fractions of total flipper length. Each cross-section is at a certain length of the flipper ('Length' (mm)) and measures different chord-lengths ('Chord' (cm)). The calculated chord-length is then used in the NACA profile63-018 (*Appendix I*) and programmed in '*Rhinoceros*' to a 3D model.

Cross-section	x	y	Distance from base (mm)	Chord-length (mm)	Model distance from base (mm)	Model chord-length (mm)
1	0.09	0.17	16.44	28.96	12.75	22.46
2	0.14	0.19	24.85	32.45	19.27	25.16
3	0.20	0.22	34.27	38.30	26.57	29.70
4	0.27	0.26	46.46	44.79	36.03	34.73
5	0.33	0.28	56.80	48.91	44.04	37.93
6	0.39	0.30	68.07	51.60	52.78	40.01
7	0.45	0.29	77.48	50.65	60.08	39.27
8	0.51	0.27	88.90	46.22	68.93	35.84
9	0.57	0.25	99.25	43.21	76.96	33.51
10	0.61	0.25	105.88	42.73	82.10	33.13
11	0.67	0.24	116.69	41.15	90.48	31.91
12	0.74	0.21	128.88	35.77	99.94	27.74
13	0.82	0.18	143.54	31.66	111.30	24.55
14	0.89	0.15	155.43	26.59	120.52	20.62
15	0.91	0.14	158.05	25.17	122.55	19.52
16	0.94	0.13	162.84	22.32	126.27	17.31
17	0.95	0.12	164.84	20.58	127.82	15.96
18	0.96	0.11	166.54	18.52	129.14	14.36
19	0.97	0.09	168.24	16.30	130.46	12.64
20	0.98	0.07	171.02	11.87	132.61	9.20
21	0.99	0.04	172.87	6.81	134.05	5.28
22	1.00	0.00	174.10	0.00	135.00	0.00

Appendix III Adelie penguin (*Pygoscelis adeliae*) free-swimming velocities and model velocities, measured at two points: 1. Base (where the flipper meets the body of the penguin), 2. Max c. (Kinematic viscosity $_{(4°C)}$ = $1.626*10^{-6}$, Kinematic viscosity $_{(20°C)}$= $1.003*10^{-6}$, flipper-length$_{true}$ = 17.41 cm, flipper-length$_{model}$=13.5cm. Rotations measured from base of the wing (rotary device radius = 5.5 cm, circum=0.345m).

Hz	Base Model (m/s)	Max c Model (m/s)	Base (m/s)	Max c (m/s)	Re Base	Re Max c
40	1.30	2.16	1.63	3.57	$2.48x10^4$	$1.13x10^5$
45	1.38	2.43	1.84	4.03	$2.80x10^4$	$1.28x10^5$
50	2.24	2.70	2.04	4.48	$3.11x10^4$	$1.42x10^5$

Appendix IV Flipper outline of Adélie penguin (*Pygoscelis adeliae*). Chord-length of the model set to model size (135mm). Maximum chord-length is found at 52mm.

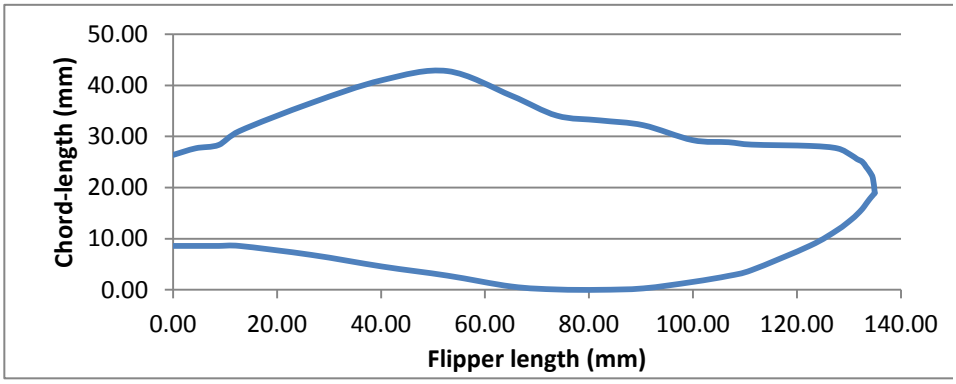

Appendix V remaining NACA-63 series for Adélie penguin flipper modeling. Each NACA profile was only used once, largest (63-040) used at the base and continuously smaller NACA profiles used towards maximum chord-length (at 52 mm).

63-020		**63-024**		**63-032**		**63-035**		**63-036**		**63-038**		**63-040**	
x	y	x	y	x	y	x	y	x	y	x	y	x	y
1,000	1,000	1,000	1,000	1,000	1,000	1,000	0,000	1,000	0,000	1,000	0,000	1,000	0,000
0,992	0,992	0,992	0,992	0,992	0,992	0,992	0,000	0,992	0,000	0,992	0,000	0,992	0,000
0,980	0,980	0,979	0,979	0,979	0,979	0,978	0,002	0,979	0,001	0,979	0,002	0,979	0,002
0,963	0,962	0,961	0,961	0,961	0,960	0,960	0,004	0,960	0,002	0,961	0,004	0,960	0,004
0,941	0,940	0,939	0,938	0,938	0,937	0,937	0,009	0,937	0,005	0,938	0,008	0,937	0,008
0,915	0,914	0,912	0,911	0,911	0,910	0,909	0,015	0,910	0,008	0,911	0,014	0,910	0,014
0,885	0,884	0,881	0,880	0,879	0,879	0,878	0,024	0,879	0,013	0,879	0,022	0,879	0,023
0,851	0,849	0,846	0,845	0,844	0,843	0,842	0,035	0,843	0,019	0,844	0,032	0,843	0,033
0,814	0,812	0,808	0,807	0,806	0,805	0,804	0,049	0,805	0,027	0,806	0,044	0,805	0,046
0,773	0,772	0,767	0,766	0,765	0,764	0,762	0,064	0,764	0,035	0,765	0,058	0,764	0,061
0,731	0,729	0,724	0,722	0,722	0,720	0,719	0,082	0,720	0,044	0,722	0,074	0,720	0,078
0,685	0,683	0,678	0,676	0,676	0,674	0,673	0,101	0,674	0,054	0,676	0,091	0,674	0,096
0,638	0,636	0,631	0,629	0,628	0,627	0,625	0,121	0,627	0,064	0,628	0,109	0,627	0,115
0,590	0,587	0,582	0,579	0,579	0,577	0,575	0,142	0,577	0,073	0,579	0,127	0,577	0,133
0,540	0,537	0,531	0,529	0,528	0,526	0,524	0,161	0,526	0,082	0,528	0,144	0,526	0,151
0,489	0,486	0,479	0,477	0,476	0,474	0,472	0,178	0,474	0,089	0,476	0,158	0,474	0,167
0,438	0,435	0,427	0,424	0,423	0,421	0,419	0,191	0,421	0,095	0,423	0,170	0,421	0,180
0,388	0,384	0,375	0,371	0,370	0,368	0,365	0,200	0,368	0,099	0,370	0,178	0,368	0,188
0,338	0,334	0,323	0,319	0,318	0,315	0,312	0,202	0,315	0,100	0,318	0,180	0,315	0,190
0,290	0,285	0,273	0,269	0,267	0,264	0,260	0,197	0,264	0,099	0,267	0,176	0,264	0,186
0,244	0,238	0,226	0,221	0,219	0,216	0,212	0,186	0,216	0,095	0,219	0,167	0,216	0,176
0,201	0,194	0,181	0,176	0,174	0,171	0,167	0,170	0,171	0,090	0,174	0,154	0,171	0,162
0,160	0,154	0,141	0,136	0,134	0,131	0,127	0,151	0,131	0,083	0,134	0,138	0,131	0,144
0,123	0,117	0,105	0,100	0,099	0,096	0,093	0,129	0,096	0,074	0,099	0,119	0,096	0,123
0,090	0,084	0,073	0,070	0,069	0,067	0,065	0,105	0,067	0,064	0,069	0,098	0,067	0,101
0,062	0,057	0,048	0,046	0,045	0,044	0,043	0,080	0,044	0,054	0,045	0,077	0,044	0,078
0,038	0,034	0,028	0,027	0,027	0,027	0,026	0,057	0,027	0,042	0,027	0,056	0,027	0,056
0,020	0,017	0,014	0,014	0,014	0,014	0,014	0,037	0,014	0,030	0,014	0,037	0,014	0,037
0,007	0,006	0,005	0,005	0,005	0,005	0,005	0,021	0,005	0,018	0,005	0,020	0,005	0,021
0,001	0,001	0,001	0,001	0,001	0,001	0,001	0,008	0,001	0,007	0,001	0,008	0,001	0,008
0,000	0,000	0,000	0,000	0,000	0,000	0,000	0,000	0,000	0,000	0,000	0,000	0,000	0,000
0,001	0,001	0,001	0,001	0,001	0,001	0,001	-0,008	0,001	-0,007	0,001	-0,008	0,001	-0,008
0,007	0,006	0,005	0,005	0,005	0,005	0,005	-0,021	0,005	-0,018	0,005	-0,020	0,005	-0,021
0,020	0,017	0,014	0,014	0,014	0,014	0,014	-0,037	0,014	-0,030	0,014	-0,037	0,014	-0,037
0,038	0,034	0,028	0,027	0,027	0,027	0,026	-0,057	0,027	-0,042	0,027	-0,056	0,027	-0,056
0,062	0,057	0,048	0,046	0,045	0,044	0,043	-0,080	0,044	-0,054	0,045	-0,077	0,044	-0,078
0,090	0,084	0,073	0,070	0,069	0,067	0,065	-0,105	0,067	-0,064	0,069	-0,098	0,067	-0,101
0,123	0,117	0,105	0,100	0,099	0,096	0,093	-0,129	0,096	-0,074	0,099	-0,119	0,096	-0,123
0,160	0,154	0,141	0,136	0,134	0,131	0,127	-0,151	0,131	-0,083	0,134	-0,138	0,131	-0,144
0,201	0,194	0,181	0,176	0,174	0,171	0,167	-0,170	0,171	-0,090	0,174	-0,154	0,171	-0,162
0,244	0,238	0,226	0,221	0,219	0,216	0,212	-0,186	0,216	-0,095	0,219	-0,167	0,216	-0,176
0,290	0,285	0,273	0,269	0,267	0,264	0,260	-0,197	0,264	-0,099	0,267	-0,176	0,264	-0,186
0,338	0,334	0,323	0,319	0,318	0,315	0,312	-0,202	0,315	-0,100	0,318	-0,180	0,315	-0,190
0,388	0,384	0,375	0,371	0,370	0,368	0,365	-0,200	0,368	-0,099	0,370	-0,178	0,368	-0,188
0,438	0,435	0,427	0,424	0,423	0,421	0,419	-0,191	0,421	-0,095	0,423	-0,170	0,421	-0,180
0,489	0,486	0,479	0,477	0,476	0,474	0,472	-0,178	0,474	-0,089	0,476	-0,158	0,474	-0,167
0,540	0,537	0,531	0,529	0,528	0,526	0,524	-0,161	0,526	-0,082	0,528	-0,144	0,526	-0,151
0,590	0,587	0,582	0,579	0,579	0,577	0,575	-0,142	0,577	-0,073	0,579	-0,127	0,577	-0,133
0,638	0,636	0,631	0,629	0,628	0,627	0,625	-0,121	0,627	-0,064	0,628	-0,109	0,627	-0,115
0,685	0,683	0,678	0,676	0,676	0,674	0,673	-0,101	0,674	-0,054	0,676	-0,091	0,674	-0,096
0,731	0,729	0,724	0,722	0,722	0,720	0,719	-0,082	0,720	-0,044	0,722	-0,074	0,720	-0,078
0,773	0,772	0,767	0,766	0,765	0,764	0,762	-0,064	0,764	-0,035	0,765	-0,058	0,764	-0,061
0,814	0,812	0,808	0,807	0,806	0,805	0,804	-0,049	0,805	-0,027	0,806	-0,044	0,805	-0,046
0,851	0,849	0,846	0,845	0,844	0,843	0,842	-0,035	0,843	-0,019	0,844	-0,032	0,843	-0,033
0,885	0,884	0,881	0,880	0,879	0,879	0,878	-0,024	0,879	-0,013	0,879	-0,022	0,879	-0,023
0,915	0,914	0,912	0,911	0,911	0,910	0,909	-0,015	0,910	-0,008	0,911	-0,014	0,910	-0,014
0,941	0,940	0,939	0,938	0,938	0,937	0,937	-0,009	0,937	-0,005	0,938	-0,008	0,937	-0,008
0,963	0,962	0,961	0,961	0,961	0,960	0,960	-0,004	0,960	-0,002	0,961	-0,004	0,960	-0,004
0,980	0,980	0,979	0,979	0,979	0,979	0,978	-0,002	0,979	-0,001	0,979	-0,002	0,979	-0,002
0,992	0,992	0,992	0,992	0,992	0,992	0,992	0,000	0,992	0,000	0,992	0,000	0,992	0,000
1,000	1,000	1,000	1,000	1,000	1,000	1,000	0,000	1,000	0,000	1,000	0,000	1,000	0,000

Appendix VII Circulation results for base rotation velocity 40Hz (blue dots) per distance from base (in m), set on the left y-axis, and the red line indicating the increase of velocity over distance from base, set on the right y-axis. Velocity would be expected to be a measure for circulation, thus an increase in velocity would lead to an increase in circulation. In this graph, however, it is proven to be otherwise. It seems that chord-length has the strongest effect on Circulation. Smallest chord-lengths are found at the base and at the wing-tip of the flipper, where in this case, low circulation values are found. As well as maximum chord-length, present at 0.052m from base, shows high circulation values.

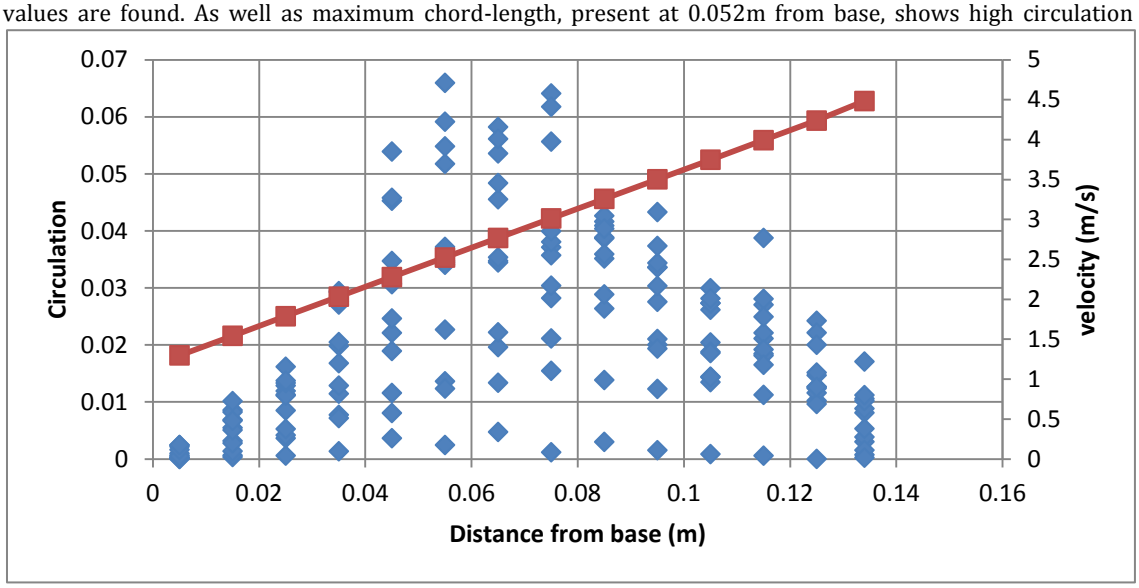

Appendix VIII Lift coefficient per base velocity rotation set to angle of attack. (Blue, red, green are average velocities of 2.90, 3.26 & 3.63 m/s resp. All three velocities show a maximum at 20°C and a minimum at 25°C. Data shows that there is a steep increase in lift between an angle of attack of 15 °C and 20°C, this could indicate the presence of an LEV. At the highest base velocity, this effect appears to be most prominent.

There is a significant difference between the three base frequencies, t-test two-sided for paired observations ($p<<0.05$). They show similar patterns in lift production as a response to increase in lift. Though the highest observational velocity, 3.63 m/s base velocity (50Hz), appears to respond strongest to this treatment. For each base velocity n=1, thus we can not conclude whether this effect is significantly different from the other base velocities. Maximum lift is reached with the highest base velocity (50Hz) and reaches 3.64, other lift values are 2.47 and 1.96 (45 and 40 Hz resp.).

The 50Hz has its second Lift peak at 30°C as opposed to both 40 and 45Hz who have their second peak at 27.5°C. The reason for this delay is not clear from our current data-set and will need further research.

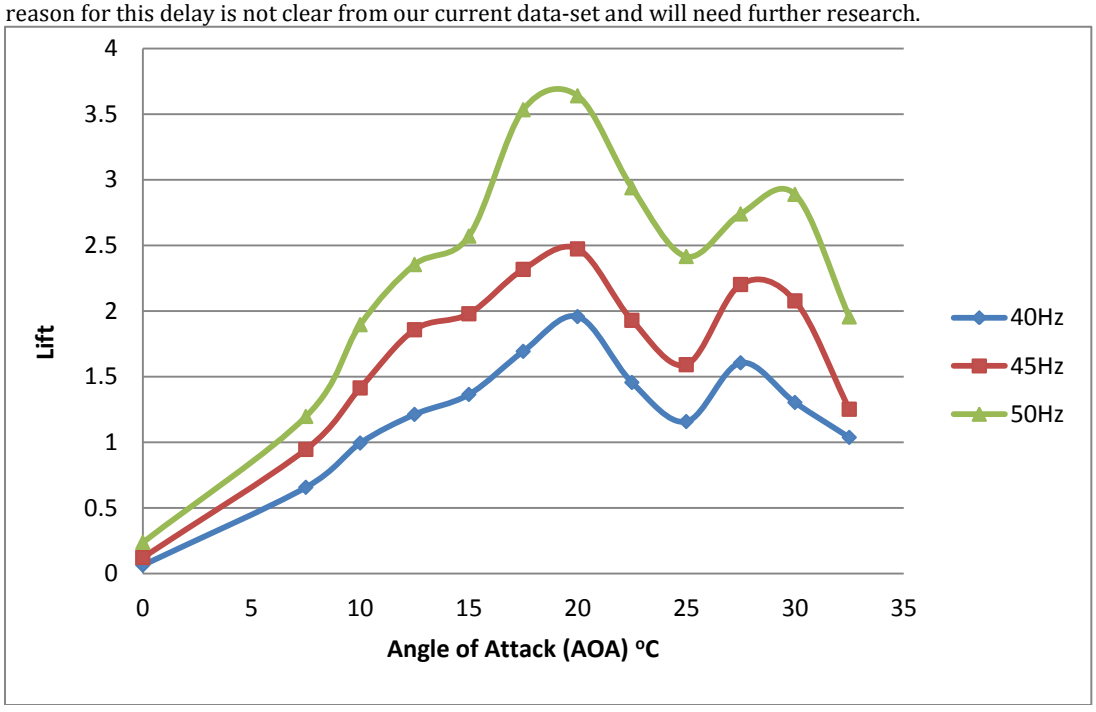

Appendix IX. Top view of the model Adélie penguin flipper in the rotary system along with the laser cross-section. The laser creates a cross-sectional view of the flow through the light reflection of the micro-particles. The flipper rotates through this cross-sectional field and the camera registers the particle movement (DPIV-analysis) which then translates and can be visualized as hydrodynamic flow around the flipper.